Surface interaction parameter measurement of solvated polymers via model end-tethered chains

Richard J. Sheridan[1], Sara V. Orski[1], Ronald L. Jones[1], Sushil K. Satija[2], and Kathryn L. Beers[1*]

[1] Material Science and Engineering Division, National Institute of Standards and Technology, Gaithersburg, MD

[2] NIST Center for Neutron Research, National Institute of Standards and Technology, Gaithersburg, MD

Abstract

We present a method for the direct measurement of the relative energy of interaction between a solvated polymer and a solid interface. By tethering linear chains covalently to the surface, we ensured the idealized and constant configuration of polymer molecules for measurement, modeling, and parameter estimation. For the case of amine-terminated polystyrene bound to a glycidoxypropyl silane film submerged in cyclohexane-d_{12}, we estimated the χ parameter for the temperature range 10.7 °C to 52.0 °C, and found a downward sloping trend that crosses the $\chi = 0.5$ threshold at 37 °C to 40 °C, in agreement with solution estimates for the same system. We simultaneously estimated the surface interaction parameter χ_s at each temperature, finding a decreasing affinity of the chains for the surface with increasing temperature, consistent with empirical observations. The theoretical model shows some limitations in a stronger solvent (toluene-d_8) that prevent rigorous parameter estimation, but we demonstrate a qualitative change

in χ and χ_s towards stronger solvency and weaker surface interaction with increasing temperature.

Introduction and Background

The interaction of dilute solvated polymers and macromolecules with the material surfaces is relevant to fields such as lithography,[1] biomedical devices,[2,3] and chromatography.[4] Indeed, the limited experimental data quantifying molecular transitions between solvation and adsorption at interfaces constitutes a fundamental barrier to improving material manufacturing in terms of quality control for complex synthetic polymers, as well as the establishment of true correlations between macromolecular structure, composition, and properties. Especially when macromolecules are used as barrier films or responsive layers in nano-structured materials and surfaces,[5] precision understanding of the surface interaction of polymers *in situ* is vital.[6]

Of particular interest is the behavior of chains during the processes of size exclusion chromatography (SEC) and interaction chromatography (IC), as well as 2D chromatographic separations, especially those involving so-called critical conditions (CC).[7] CC chromatography is generally characterized as an intermediate between SEC and IC, where enthalpic attractions balance entropic repulsions, the free energy of adsorption becomes zero, and elution occurs in a molecular mass independent fashion. Guttmann *et al.* have presented a model that can reproduce, across all these regimes, the elution curves of a polymer given the polymer's structure.[8] This model has recently been extended to operate at a nearly atomistic level of detail.[9,10] The ability to extend and experimentally apply these models to new polymer structures would represent an immediate catalyst to method development in interaction based separations for synthetic polymers, and broaden adoption of this promising method of macromolecular characterization.

In Guttmann's model, the partition function for isolated chains in a pore is calculated via a Di Marzio-Rubin[11] lattice model, and is used to predict elution curves via the Casassa[12] method. This model has only one free parameter χ_{s}, which is the dimensionless relative interaction energy between a segment and the pore wall:

$$\chi_{\mathrm{s}} = \left(u_{\mathrm{wp}} - u_{\mathrm{wm}}\right)/kT \qquad (1)$$

In eq 1, u_{wp} is the potential energy of a polymer-surface contact, u_{wm} is the potential energy of a monomeric solvent-wall contact, k is the Boltzmann constant, and T is the system temperature. This χ_s is somewhat different from the χ parameter from Flory-Huggins solution theory:

$$\chi_{\mathrm{pm}} = z\left[u_{\mathrm{pm}} - \tfrac{1}{2}\left(u_{\mathrm{pp}} + u_{\mathrm{mm}}\right)\right]/kT \qquad (2)$$

where z is the connectivity of the lattice, u_{pm} is the energy of a polymer-solvent contact, and u_{pp} and u_{mm} are the self-contact energies for polymer and solvent, respectively. The surface interaction energy can be written, if desired, in terms of "wall χ", treating the solid phase as just another species:

$$\chi_{\mathrm{s}} = \tfrac{1}{z}\left(\chi_{\mathrm{wp}} - \chi_{\mathrm{wm}}\right) \qquad (3)$$

By adjusting this surface interaction parameter, one can calculate chromatographic peak elution volumes that coincide with those observed by experiment, such as in the data generated by Pasch.[7,13–15] Although the parameter is a pure interaction energy within the model, it effectively encapsulates real effects such as the solvent quality and the shape of the pore, as well as any number of unknown effects, much like χ abstracts entropic and virial contributions to solvent quality. The Guttmann model is therefore currently useful only as an explanatory tool rather than a predictive tool, unless some external method to measure the interaction energy is used. With an external estimate of the interaction energy, the magnitude of any encapsulated

effects can be determined. In this work, we attempt to measure this interaction energy as directly as possible. This involves a new application of physics-based modeling to an area of polymer science that is rife with quasi-empirical formulas, and strengthening the connection of physics and macromolecular metrology.

A fundamental problem exists in the measurement of the chromatographic polymer-surface interaction energy, or indeed anything involving the configuration of polymer chains as they partition into the pores of a chromatographic column. Namely, these systems are extremely dilute and we are interested mainly in the conformation of individual species undergoing adsorption or confinement. By increasing concentration, detectible differences might become apparent using some highly sensitive instrumentation (e.g. small angle neutron scattering (SANS) or quartz crystal microbalance (QCM)); however, at those conditions the concentration is too high to be directly comparable to chromatographic conditions and energetics. For these reasons, the literature contains few quantitative measurements of the interaction energy that are transferrable to method development in this area of measurement science.[16,17]

Only two experimental measurement techniques have shown real promise in detecting macromolecular configuration on the length and size scales of interest here: SANS and Neutron Reflectivity (NR). Cosgrove measured the amount[18,19] and configuration of poly(ethylene oxide) chains adsorbed from heavy water on polystyrene latex, as well as polystyrene end-tethered to silica microparticles, with SANS. They compared experimental data with predictions from lattice-based Monte Carlo and self-consistent field theory models in a semi-quantitative manner. In strong solvents like N,N'-dimethylformamide-d_7 or toluene-d_8, the scattering patterns from the polystyrene film indicated the presence of an enriched layer of solvent near the surface, while in cyclohexane-d_{12} the near-surface region is depleted of solvent. Mansfield *et al.* later performed a

neutron reflectivity experiment on a comparable system, swelling end-tethered polystyrene in deuterated cyclohexane and toluene.[20] Their observations agreed with Cosgrove's, with solvent enrichment in toluene and solvent depletion in cyclohexane. While the Mansfield study could produce quantitative fits of their layer models to their reflectivity curves, they only qualitatively compare their result to physical models of end-tethered polymer behavior. Furthermore, their films were grafted only with an associative COOH-SiO_2 bond (16 kJ/mol)[20] that cannot guarantee constant grafting density of the films, neither between solvents, nor within several measurements in the same solvent. Some of the most comprehensive studies of end-tethered polymers, including observations of surface interaction were performed by Kent.[51] However, the fact that the measurement is performed at an air-liquid interface limits applicability for our purposes.

In the following experiment, we produced an end-tethered polystyrene film (PSN) with a sufficiently low grafting density to reveal the surface interactions observed by Cosgrove. This solves the challenges posed by the direct measurement of free chains, without totally masking the conformational changes due to surface interaction. This low grafting density was achieved using a high-temperature "grafting-to" approach, where primary-amine terminated polystyrene was spin-coated over a silicon wafer bearing a sub-monolayer of epoxide-functionalized silanes and then heated to ensure covalent grafting. We then measured the neutron reflectivity profile of the film swollen in solvent.

Neutron reflectivity profiles are usually interpreted through the lens of simple slab models, often with roughness approximations for each interface. However, end-tethered polymers and other soft swollen films often have complex shapes that require many such slab layers to adequately model, leading to a complex model with many covarying parameters that provide

little insight into the physics of the film. A theoretically informed model is more appropriate for such materials. The parabolic segment density profile for ideal polymer brushes[21–23] is a classic example of this idea, but because it does not include the surface interaction behavior of the chains, it is not suitable for our purposes. Likewise, a quasi-analytical model for isolated chains[24] provides a segment density profile, but one that does not include the interchain interactions that exist in our finite-grafting-density films. The Scheutjens-Fleer numerical self-consistent field theory (SF-nSCFT)[25–27] avoids these issues at the cost of numerical approximation. This formalism is an appropriate choice, since it includes surface, solvent,and interchain interactions. Furthermore, like the Di Marzio-Rubin model underlying Guttman's chromatography model, it is a lattice-based model. Therefore, the surface interaction parameter of our model should be directly comparable to the surface interaction energy of their model.

We chose to fit our reflectivity curves using the thermodynamic parameters of the SF-nSCFT, and showed that in the case of moderate solvent quality and attractive surface interaction (cyclohexane-d_{12}), the surface interaction parameter can be measured with significant precision. (We use the term "precision" deliberately, see the Appendix for further discussion.) We also showed that there is some discrepancy between the model and reflectivity observations in a high solvent quality, repulsive surface interaction system (toluene-d_8), and propose some causes and potential solutions that may enable surface interaction parameter measurements for these systems in the future.

Materials and Methods

End-tethered polymer film synthesis

Amine-terminated polystyrene, PSN, (number average molar mass M_n = 25 kg/mol, weight average molar mass M_w = 26 kg/mol) was purchased from Polymer Source, Inc. Cyclohexane-d_{12} and toluene-d_8 were purchased from Cambridge Isotope Laboratory. 100 mm x 12 mm N-

doped silicon wafers were ordered from University Wafer. The silicon wafers were used from a freshly chemically mechanically polished state to ensure Angstrom smoothness of the interface; root mean square roughness was 5.4 Å as measured via atomic force microscopy on a Bruker Icon in tapping mode with TAP525A probe. (3-Glycidoxypropyl) dimethylethoxysilane (GPDMEOS) and pyridine were obtained from Sigma Aldrich. The wafers were treated with ultraviolet/ozone (UVO) in a Jelight UVO Cleaner model 342 for 30 min, then placed in a reaction cell and heated to 50 °C with a solution of pyridine and GPDMEOS in toluene ($1{:}10{:}10^4$ by volume.) This reaction was halted after 24 h, and the wafer was subjected to a rinse cycle (toluene, ethanol, and then deionized water) and further Soxhlet extraction in toluene followed by another rinse cycle and drying with nitrogen. A 1 % by mass solution of PSN dissolved in toluene was spin-cast on to the wafer, which was then baked at 150 °C for 24 h to ensure sufficient grafting of the amine end-groups to the epoxide-bearing surface.[28] To ensure the removal of all physically adsorbed chains, the wafer was rinsed with toluene, DMF, and acetone before being subjected to three days of Soxhlet extraction in toluene followed by another rinse with DMF, toluene, ethanol, and deionized water. This rigorous cleaning process is necessary because we and others[29] have observed stubborn layers of physisorbed chains forming over the 24 hour baking process. After the first and second days of Soxhlet extraction, we observed a decrease in ellipsometric thickness from the previous day, while over the third day less than an Angstrom of material was lost. The cleaned wafer was dried in a vacuum oven at 150 °C for 4 h, then measured by NR in its dry state, and finally sealed in the liquid reflectivity cell. To change solvents, the previous solvent was removed by pipette, and the chamber was dried with a stream of dry nitrogen until no visible solvent droplets or films remained, then the new solvent was inserted into the chamber.

Neutron reflectivity data reduction and modeling

The raw data collected by the NG7 reflectometer were reduced using reflred, a program in the reflpak suite.[30] The reduced data were modeled using layer models in Refl1D.[31] The dry films were modeled as simple Material stacks with roughness. The swollen films, because their reflectivity signals are fringeless, were modeled using the EndTetheredPolymer layer, which is driven by an implementation of the Scheutjens-Fleer numerical self-consistent field theory[25–27] created in support of this project. In addition to the description of the formalism in the appendix, we note that this field theory code is a synthesis of the work of Cosgrove[32] and De Vos,[33] and that the source code is available with the Refl1D software package.[31] Fitting scripts and reduced data have been provided in the Supporting Information.

Small Angle Neutron Scattering data reduction and modeling

PSN was dissolved in cyclohexane-d_{12} and toluene-d_8 at a concentration of 1 mg/mL. This solution was transferred into titanium cells with quartz windows 25 mm in diameter and spaced 0.4 mm apart. These were taken to the NIST Center for Neutron Research (NCNR) NGB beamline and placed in a temperature-controlled sample rack. The raw data collected by the NGB 10 m SANS detector were reduced using NCNR SANS reduction macros[34] running on Igor Pro 6.37 by Wavemetrics. This work benefitted from SasView[35] software, originally developed by the DANSE project under NSF award DMR-0520547. The model used was the "polymer excluded volume" model capturing the radius of gyration R_g and Flory exponent ν with a single quasi-analytical form,[36] over the Q range 0.009 Å^{-1} to 0.5245 Å^{-1}.

Spectroscopic Ellipsometry

Thickness monitoring for the effectiveness of Soxhlet extraction of physisorbed chains was performed using spectroscopic ellipsometry (SE). Spectral scans from 200 nm to 1000 nm (2000 Å to 10000 Å) were collected at an incident angle of 65° on a J. A. Woolam M2000 with

automatic stage movement and sample alignment. To measure the PSN film on the wafer in this study, thicknesses for the SiO_2 and GPDMEOS layers were collected from comparable wafers and used as fixed layers when measuring the PSN film thickness. The refractive index for SiO_2 was modeled with Woolam's native oxide material parameters, for PSN was modeled using Woolam's polystyrene material parameters, and GPDMEOS was assumed to behave as a Cauchy model with parameters $A = 1.45$, $B = 0.01$, $C = 0$. A 1 mm spaced grid of measurements over the entire wafer surface were collected as a single ellipsometric map of the film thickness. The PSN film measured 63 Å ± 7 Å after 24 h of Soxhlet extraction followed by 4 h of vacuum annealing at 150 °C, and 48 ± 5 Å after 48 h, and 47 Å (single point measurement, not a map) after 72 h.

Results and Discussion

Dry film and substrate analysis

To build a complete layer model of a swollen end-tethered polymer film, it is necessary to first specify the material parameters of the silicon substrate. For very thick films, these parameters can be ignored or coarsely estimated. In our case, the structure of our swollen film is on the same size and contrast scales as the substrate, so we rigorously measured the neutron reflectivity profile of our polystyrene film in a dry, annealed state. Additionally, we measured the neutron reflectivity profile $R(Q)$ of another identical silicon substrate coated with an identical epoxy-silane sub-monolayer. These reflectivity profiles were fitted simultaneously, specifying that the roughnesses of the interfaces of the silicon and native silicon oxide (SiO_2) materials should be in accordance with literature expectations,[37] and the roughness of the SiO_2/GPDMEOS interface corresponds to RMS roughness measurements on an atomic force microscope. The densities of silicon, SiO_2, and polystyrene were taken from literature, leaving the scattering length density and porosity of the GPDMEOS layer, as well as the thickness and roughness of both GPDMEOS

and PSN layers, and finally the intensity and angle offset instrumental parameters as fitting parameters. The specification of all these parameters enables a precision of measurement in the fitted parameters that would normally be unachievable through the direct fitting of all parameters. The resulting data and scattering length density fits $\rho(z)$ are presented in Figure 1 and Figure 2. The fits produced the necessary parameters, presented in Table 1, to feed forward into our analysis of the swollen PSN films, as well as giving a measurement of the dry thickness of the PSN film at 34.06 Å ± 0.74 Å. This implies a grafting density σ of 0.088 nm^{-2} (0.00088 Å^{-2}) or a reduced grafting density $\Sigma = \sigma\pi R_g^2$ of 8.6 (taking the radius of gyration R_g = 55.8 Å from Figure 8.)

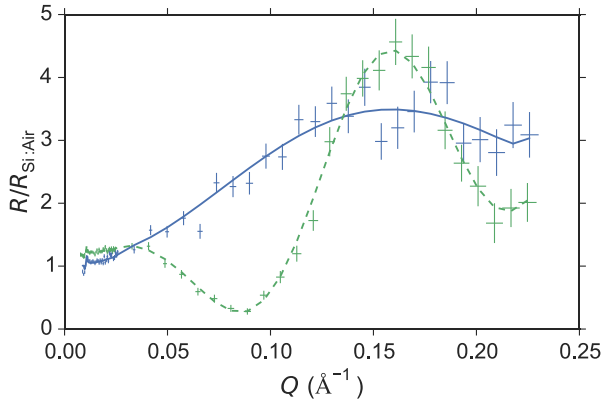

Figure 1. Neutron reflectivity data (crosses) and best-fit modeled curves (lines) for GPDMEOS (blue) and PSN/GPDMEOS (green, dashed) films on silicon substrates in air. All points have been normalized by the theoretical reflectivity of a perfectly flat silicon surface (the so-called Fresnel reflectivity.) The curves are fit simultaneously to reveal the structure of the collapsed end-tethered film. The size of the crosses represents one standard deviation of uncertainty in the reflectivity signal according to Poisson counting statistics (vertical) and wavelength smearing (horizontal).

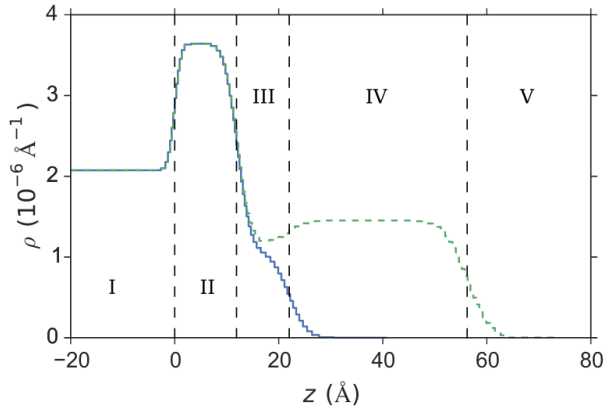

Figure 2. Scattering length density curves corresponding to the best-fit dry film models for GPDMEOS (blue, solid) and PSN/GPDMEOS (green, dashed) films on silicon substrates in air as in Figure 1. The five modeled layers are separated by vertical dashed lines: (I) silicon, (II) silicon dioxide, (III) GPDMEOS, (IV) PSN (green, dashed only), (V) air. The blockiness of the models is due to the choice of step size in the discretization scheme used for the Abeles matrix reflectivity calculation.[31,38]

Table 1. Fitted substrate parameters from the GPDMEOS and PSN/GPDMEOS multifit analysis.

Parameter	Value	Unit
h_{PS}	34.06 ± 0.74	Å
h_G	10.01 ± 0.67	Å
h_{SiO_2}	12.06 ± 0.24	Å
ρ_G	1.162 ± 0.049	10^{-6} Å^{-1}
r_{PS}	3.27 ± 0.74	Å
r_G	2.2 ± 1.4	Å
φ_G	13.4 ± 9.1	%

The layer structure shown in Figure 2 is complicated enough to benefit from some additional explanation. The substrate layer (I) is modeled as pure silicon with the literature values for

atomic composition and density. The native silicon oxide layer (II) is modeled as pure silicon dioxide with the literature density for an amorphous structure. Any variation in the atomic composition in the real film is largely captured by the interfacial roughness parameters. The GPDMEOS layer (III) is modeled as an empirical scattering length density (SLD) due to the unknown degree of reaction of the methoxysilane groups, and with a percentage of void volume to capture any porosity and small scale sparsity of the layer. The SLD is lower than other components of the film; this is likely due to the relatively high concentration of protons per unit mass in the layer originating from the glycidoxypropyl group. The voids are defined in such a way that air, polystyrene, or solvent are allowed to completely fill them. The PSN layer (IV) is modeled as an independent organic layer, existing in only one of the two simultaneously fitted models. The air layer (V) takes up the space of (IV) for the model where PSN is not present. We note that each of these choices has a physical basis and produces a noticeable difference in quality of fit.

Cyclohexane-d_{12} swollen film analysis

Following the measurement of substrate parameters, the silicon wafer bearing the PSN end-tethered film was enclosed in a temperature-controlled, sealed environmental cell which was then filled with fresh cyclohexane-d_{12}. This cell places the back face of the wafer in contact with a computer-controlled recirculating bath, allowing us to automatically collect backside reflectivity profiles of the swollen PSN film at a range of temperatures, from 10.7 °C to 52.0 °C. Representative data and corresponding model fits are presented in Figure 3 and Figure 4.

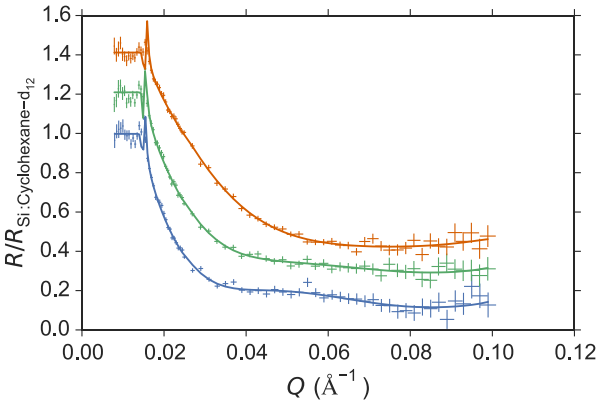

Figure 3. Reflectivity data (crosses) and best fit models (lines) of the PSN end-tethered film swollen in cyclohexane-d_{12} at 10.7 °C (red), 34.2 °C (green), and 52.0 °C (blue). All points have been normalized by the theoretical reflectivity of a perfectly flat silicon surface in contact with cyclohexane-d_{12}, then shifted vertically for visibility. As temperature increases, the central peak around 0.06 Å^{-1} appears and the initial slope beyond the critical Q steepens. The SF-nSCFT model follows these changes across the whole measured Q range. The size of the crosses represents one standard deviation of uncertainty in the reflectivity signal according to Poisson counting statistics (vertical) and wavelength smearing (horizontal).

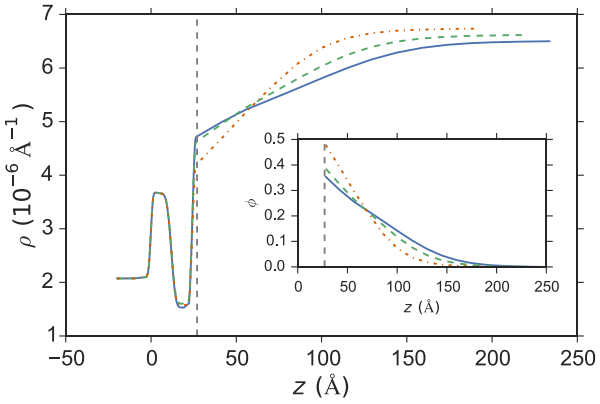

Figure 4. Scattering length density curves of PSN end-tethered films swollen in cyclohexane-d_{12} at 10.7 °C (red dashed), 34.2 °C (green dashed), and 52.0 °C (blue) corresponding to the best fit models of Figure 3. The origin of the z coordinate is defined by the location of the silicon

substrate interface. The film (right side of black dashed line) is observed to increase in scattering length density ρ after the solid interface (left side of black dashed line) but with decreasing slope as temperature increases. Inset is the corresponding inferred volume fraction of polystyrene.

In Figure 3, subtle but clear differences in the behavior of the films are apparent. At the lowest temperature (10.7 °C,) there is a featureless reflectivity profile reminiscent of what might be expected from a simple sigmoidal "rough" interface. At the highest temperature (52.0 °C,) there is one weak fringe around 0.06 $Å^{-1}$ in the reflectivity profile and a steeper slope near the critical angle. At intermediate temperatures, the reflectivity curve takes an intermediate form between these two. There is a slight upturn to the curves in the noise around 0.1 $Å^{-1}$ due to the combined contributions of the substrate layers. This demonstrates the impossibility of fitting the detailed structure of the substrate without the *ex situ* measurements of the previous section.

We interpret these reflectivity shifts through the SF-nSCFT and reflectivity models as the collapsing and swelling of the PSN chains as the solvent quality of cyclohexane-d_{12} changes with temperature. At low temperature, the polymer segments are largely collapsed near the surface with relatively few tails reaching a short distance away from the substrate. As the temperature increases, polymer segments swell away from the surface and the tails can reach farther into the solution.

Because we have fixed many parameters using the values from the dry film measurements, the overall reflectivity model has seven fitting parameters: Two instrumental parameters, the intensity and angle offset of the neutron beam, which are fit precisely and without correlation with other parameters; two interaction parameters, the polymer-solvent interaction parameter χ and the net polymer-surface interaction χ_S; and three material parameters, the volume fraction of pores in the GPDMEOS layer φ_G, the amount of polymer grafted to the surface in terms of the

dry thickness h_{dry}, and the dispersity of the tethered polymer chains, $Đ$. h_{dry} is a dimensionally convenient proxy for the mass of grafted polymer material; it is the hypothetical thickness of the modeled film if it were totally collapsed ("dry"), despite the fact that the model reflects solvated conditions. The reason for fitting these material parameters was to determine their extent of correlation and run-to-run variation of the fitted value. While we found that φ_G was consistent with (and in fact more precisely estimated than) the value found from dry film measurements, under the conditions of the cyclohexane temperature series, we found that the data collected had no power to determine $Đ$, despite the strong influence dispersity can have on the polymer volume fraction profile.[33] Furthermore, the substantial parameter correlation between $Đ$ and χ, χ_s, and h_{dry}, meant that the uncertainty of all our SF-nSCFT parameter estimates were broadened (See Figure S7 in the Supporting information.)

When the dispersity is fixed to an externally measured value, 1.06 as reported by the manufacturer, measured by size-exclusion chromatography, the precision of the parameter estimates improves markedly (See Figure S8 in the Supporting information.) We again found φ_G to be consistent with the dry PSN film. The value of h_{dry} was consistent across temperatures; however, the value necessary to fit the data to be about 10 Å less (h_{dry} = 24 Å, σ = 0.062 nm^{-2} (0.00062 Å^{-2}), Σ = 6.1) than the h_{PS} we observed from the dry film measurements. This discrepancy is large in a relative sense because it is a large fraction of the total polymer film thickness, but small in an absolute sense, because the possibility exists for a nanometer of hydrocarbon material to either adsorb before the solvent-free measurement or desorb just before the solvated measurement. Additionally, this h_{dry} value is computed indirectly through the SF-nSCFT, so there may be a discrepancy between reality and the way distances and masses are handled in that theory (see the Appendix for more discussion.)

With this caveat in mind, we now turn to the desired measurement of the system, the interaction parameters χ and χ_s. These values are plotted in Figure 5 as a function of temperature. χ decreases with increasing temperature, meaning solvent quality or strength increases, passing through the theta point $\chi = 0.5$ at 37 °C to 40 °C. χ_s decreases with increasing temperature, meaning the strength of interaction of the polymer with the wall decreases, although the magnitude of the χ_s parameter greater than 0.18 (a theoretical adsorption transition point in the SF-nSCFT) across the entire measured temperature range. This means we observe strongly attractive behavior even at our highest experimental temperature. These observations of χ and χ_s are in strong agreement with empirical expectations. Polystyrene is known from neutron scattering experiments to have a theta temperature in cyclohexane of 35 °C and 38 °C to 40 °C in cyclohexane-d_{12}.[39] Polystyrene is also known to form films on silicon that are practically impossible to wash away with cyclohexane.[40] Figure 5 demonstrates that, by following the protocol laid out in this work, one can obtain a measurement of the surface interaction parameter χ_s for a given polymer-solvent-surface system. The uncertainty of the χ_s parameter estimate is only mildly correlated with the uncertainty of the polymer-solvent interaction parameter χ (see Figure S8 in the Supporting Information)

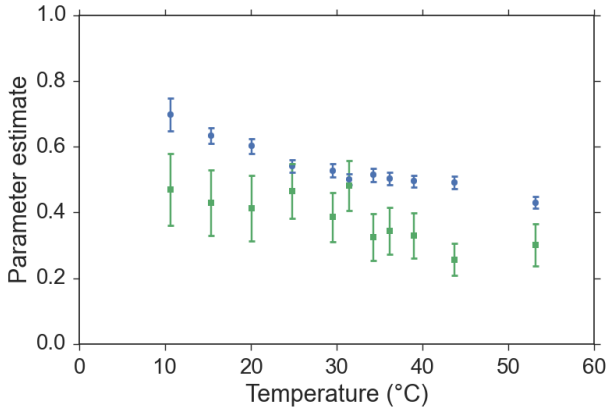

Figure 5. χ (blue circles) and χ_s (green squares) of polystyrene in cyclohexane-d_{12} via the SF-nSCFT model as a function of temperature. χ decreases with temperature indicating increasing solvent quality. χ_s decreases with temperature indicating decreasing polymer-surface interaction.

Table 2. Temperature-independent parameters for the PSN-cyclohexane-d_{12} temperature series, as a weighted average across measurements.

Parameter	Value	Unit
h_{dry}	24.5 ± 1.3	Å
φ_G	11.3 ± 2.7	%

Toluene-d_8 swollen film analysis

The same PSN film was subsequently dried with a stream of nitrogen gas and then submerged in fresh toluene-d_8. The neutron reflectivity curve collected from this system at 22 °C, pictured as a solid line in Figure 6, is qualitatively different from even the hottest cyclohexane-d_{12} measurement. The central fringe is relatively large, narrow, and peaks at lower Q, indicating a film which is of a relatively larger size and more uniform SLD composition. Unfortunately, the same set of fitting parameters which worked so well in the cyclohexane-d_{12} series could not capture all the features of the reflectivity curve. The "best fit" SLD profile in toluene-d_8 is shown with the solid line in Figure 7.

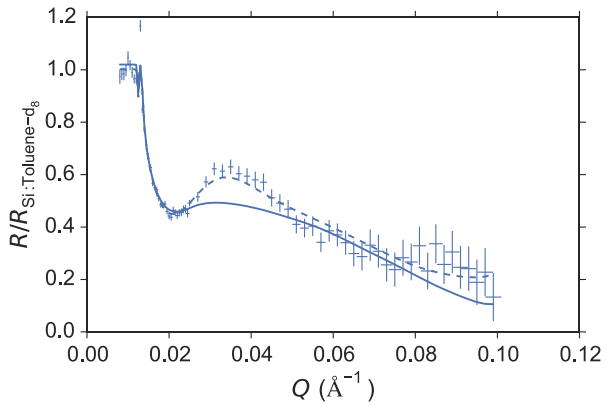

Figure 6. Reflectivity data (crosses) and best fit model (solid line) of the PSN end-tethered film swollen in toluene-d_8. The optimization of this set of parameters clearly leads to a poor fit, with systematic deviations from the data near the important fringe. The best fit model including lattice

parameters (dashed line) has two additional parameters permitting a significantly tighter agreement between the model and data.

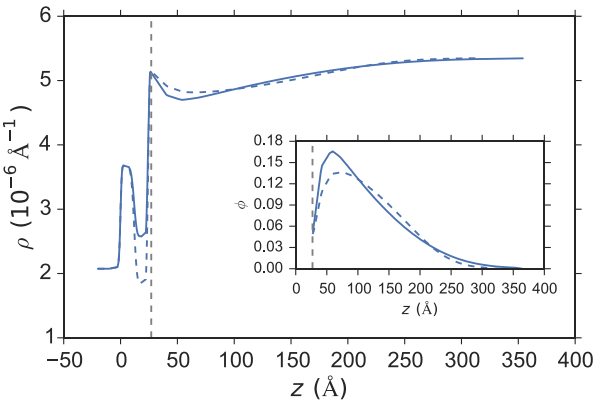

Figure 7. Scattering length density curves of the PSN end-tethered film swollen in toluene-d_8 at 22.0 °C, corresponding to the best fit model without (solid) and with (dashed) additional lattice fitting parameters of Figure 6. Although the model should not be taken as a quantitative representation of the film structure, it shows qualitatively an expansion of the end of the film and a solvent enrichment layer near the surface compared to the cyclohexane-d_{12} results in Figure 4.

Table 3. Parameters corresponding to the best fit model of the PSN end-tethered film swollen in toluene-d_8, shown in Figure 6 and Figure 7 as a solid line.

Parameter	Value	Unit
h_{dry}	19.98 ± 0.33	Å
χ	0.0066 ± 0.0067	
χ_s	-0.965 ± 0.032	
φ_G	33.42 ± 0.48	%
$Đ$	1.296 ± 0.022	

Clearly, the parameters for this fit are not to be viewed as realistic or predictive estimates. Rather they demonstrate that the optimizer is struggling to fit the data by driving the parameters to their extremes of repulsive surface interaction and high solvation power. This could be a consequence of the redimensionalization scheme which allows the lattice-based SF-nSCFT to be mapped on to real spatial dimensions (see the Appendix for details). The length and the amount of polymer mass that can be contained in a lattice segment is defined based on the dimensions of pure random walks. However, polymers in good solvents are known to follow a self-avoiding random walk.[39] One way to coarsely allow the model to expand the polymer chain is to allow these lattice parameters m_l = 590 g/mol and l_l = 14.2 Å (the mass and length of a lattice segment, respectively) to be optimized in the fit as well, although they are meant to have a strictly defined value based on external measurements.[27] The fit to the data with these extra parameters is presented in Figure 6 and Figure 7 as dashed curves (see Table S1 for values). These additional parameters allow the optimizer to find a model which more closely tracks the reflectivity data. While we still cannot interpret the parameters quantitatively, the resultant SLD profile continues to show solvent enrichment near the substrate, indicating a strongly repulsive surface interaction between this interface and polystyrene in a strong solvent.

Small angle neutron scattering comparison

As a central question of this study is the solvation and dimensions of the end-tethered PSN film, we performed a SANS study with comparable materials and conditions to our neutron reflectivity results. PSN was dissolved in cyclohexane-d_{12} and toluene-d_8 at 1 mg/mL, sufficiently dilute to avoid any inter-chain interaction. The polymer excluded volume model fits are plotted against the reduced, radially integrated SANS data in Figure 8. The estimated radius of gyration (R_g) for each measurement across the temperature range of interest is plotted in

Figure 9 and the corresponding Flory exponent ν (the fractal dimension of the mass distribution of the chain, $R_g \propto M_n^{\nu}$) plotted in Figure 10.

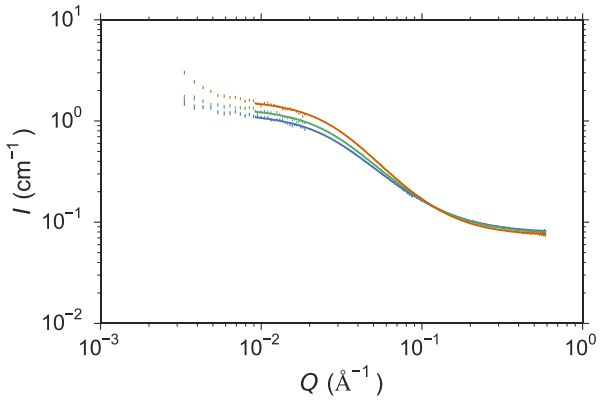

Figure 8. Comparison of scattering intensity of free PSN in cyclohexane-d_{12} at 50 °C (blue), 35 °C (green), and 15 °C (red) to model fits. Chi-squared statistics for the fits are generally around 2. Horizontal errorbars have been omitted for clarity.

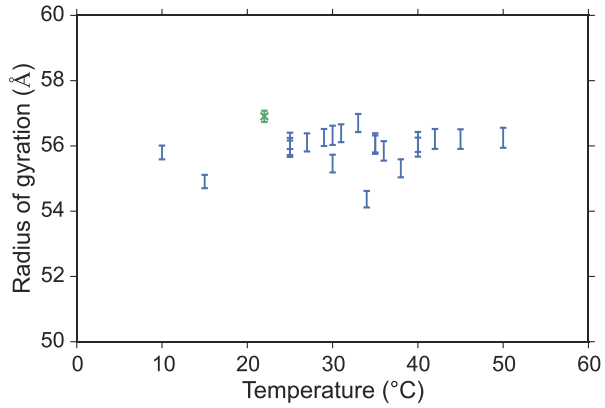

Figure 9. Radius of gyration of PSN in cyclohexane-d_{12} (blue bars) and toluene-d_8 (green cross) as a function of temperature. The size of the error bars is one standard deviation of the parameter estimate. Although there is an upward-sloping trend in the data, all the points in cyclohexane-d_{12} are within experimental variability of each other with a weighted average of 55.8 Å.

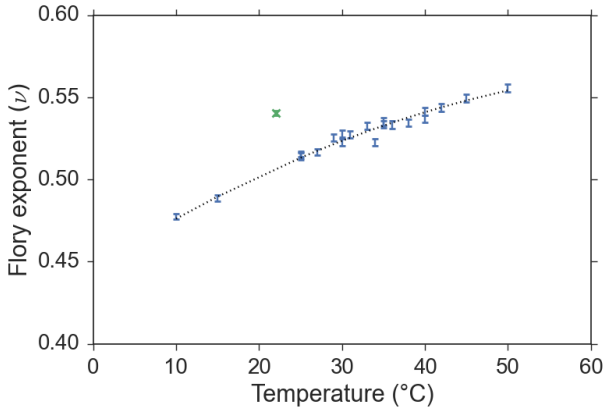

Figure 10. Flory exponent of PSN in cyclohexane-d_{12} (blue bars) and toluene-d_8 (green cross) as a function of temperature. The upward-sloping trend agrees with expectations, however there is a shift placing $\nu = 0.5$ (the value for a Gaussian coil) at about 20 °C, rather than the literature theta temperature of 38 °C. The dotted curve is a quadratic fit to the cyclohexane-d_{12} data serving as a guide to the eye.

The modeled radius of gyration for PSN does not show any strong temperature dependence in cyclohexane-d_{12}. The measurement in toluene-d_8 is higher, but within the experimental scatter of the cyclohexane-d_{12} data. This lack of temperature and solvency dependence is consistent with the relatively short PSN chain length.[41] It is a stark contrast, however, to the strong temperature dependence of the measured Flory exponent. The value of ν is the fractal dimension of the mass distribution within the chain, and takes a value of 0.5 for Gaussian chains, 0.588 for self-avoiding chains, and 1/3 for collapsed chains. In this sense, the data agrees with the χ observed in the neutron reflectivity experiment for solvent strength (Figure 5). This curve is offset from our measurements of χ, however, as it reports $\nu = 0.5$ at approximately 20 °C, compared to the 35 °C to 40 °C range where $\chi \approx 0.5$. We do not have a concrete explanation for this discrepancy, although we speculate it is related to the free amine end group, which may have a relatively large effect at this chain length (M_n = 25 kg/mol).

If we take the weighted average radius of gyration in cyclohexane (55.8 Å) as a measure of the unperturbed dimensions of the tethered chains as if they were in solution, we may construct a curve of the expansion ratio r_{ex} of the film as a function of temperature using the root mean square layer thickness h_{RMS}, which can be calculated from the polymer volume fraction as a function of distance from the interface $\phi(z)$:

$$r_{\mathrm{ex}} = \frac{h_{\mathrm{RMS}}}{R_{\mathrm{g}}} = \frac{1}{55.8\ \text{Å}} \sqrt{\frac{\int z^2 \phi(z) dz}{\int \phi(z) dz}} \qquad (4)$$

Plotting this at each temperature, we construct Figure 11.

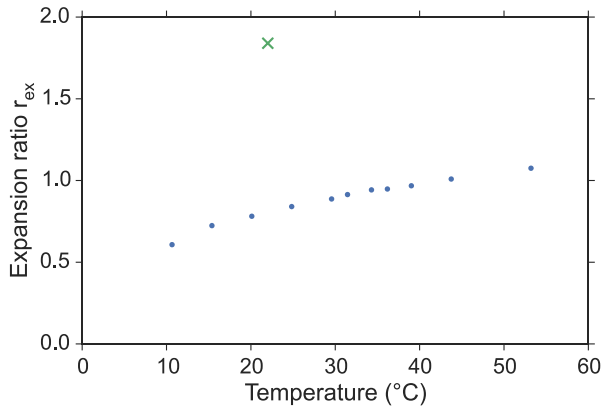

Figure 11. PSN film expansion ratio in cyclohexane-d_{12} (blue dots) and toluene-d_8 (green cross) as a function of temperature. The film is in a collapsed state even above the theta temperature. The high expansion ratio in toluene is largely due to contributions from confinement to the interface and the surface interaction parameter χ_s.

We note two important features of Figure 11. First, the r_{ex} for our PSN film in cyclohexane-d_{12} is less than one at low temperature and increases with temperature, approaching unity near the temperature where $\chi \approx 0.5$. This is on the order of renormalization group theory predictions[24] for isolated tethered chains and below Kent's[42,51] observations for sub-brush films, despite a reduced grafting density Σ of 6 – 8. Second, r_{ex} in toluene-d_8 is expanded more than would be

expected for an isolated chain attached to a repulsive surface (1.84 *versus* 1.47) but on the order of reported brush data. These two points are a consequence of the surface interaction; while the higher-than-mushroom grafting density of the PSN film partially occludes the surface interaction, there is sufficient response not only in the details of the segment density profile, but also in aggregate properties like r_{ex}. Given a sufficiently predictive model of end-tethered polymers, it may be possible to infer surface interaction quantitatively in r_{ex} or other aggregate properties that are measurable with common techniques such as ellipsometry.

Conclusion

A method was presented to measure the thermodynamic surface interaction parameter χ_{s}, as well as the Flory-Huggins solvent interaction parameter χ, in one experiment using a carefully prepared end-tethered polymer film. Neutron reflectivity data of the film swollen in solvent was collected and a layer model was directly fit with parameters of a self-consistent field theory, allowing for the generation of parameter estimates and uncertainty derived directly from the instrument measurement uncertainties. The temperature dependence of χ and χ_{s} in cyclohexane-d_{12} was observed and demonstrated agreement with previously reported work. The method was less successful in describing the system swollen in toluene-d_8. More parameters were added to create a SLD profile that empirically matched the observed reflectivity data, showing a substantial solvent enrichment zone near the substrate interface which indicates a repulsive surface interaction. The neutron reflectivity measurements were more sensitive to the nanoscale configurational changes of the end-tethered film than classic SANS measurements of free chains for these short polymer chain lengths, with an amplified effect from confinement and surface interaction on chain dimensions as demonstrated through calculations of r_{ex} and h_{RMS}.

Future experiments of this kind should include solvent-polymer-surface systems that have been explored in the critical chromatography literature. These types of systems present a challenge, both in terms of creating a surface with sufficient reactive groups that yet is comparable to a chromatography column packing, and in modeling of the mixed-solvent systems that are typically used in lieu of temperature control as we have used in the present work. This experiment pushed the limits of the neutron reflectivity technique, requiring Angstrom smoothness and macroscopic uniformity of film properties, and was ultimately limited by incoherent background scattering noise and accuracy of the theory describing the nanoscale configuration of the film. Additionally, some correction to the SF-nSCFT formalism or code should be introduced that will allow a quantitative fit to strongly-solvated polymer systems. Otherwise, a more general alternative model such as molecular dynamics or lattice Monte Carlo simulations should be applied to better capture the self-avoiding behavior of the tethered chains and avoid the mean-field approximations inherent in SCFT.

Acknowledgements

The authors would like to thank Frédéric Restagno for helpful discussions that improved the end-tethered polymer film synthesis. The authors also thank Guangcui Yuan for a generous donation of beam time as well as supporting the operation of the NG7 beamline. The authors also acknowledge the nSoft consortium for providing access to the NGB 10m SANS instrument. The authors thank Amanda McDermott for support in the collection of SANS data, and Jon Seppala for assistance in the reduction and analysis of SANS data.

Associated Content

Supporting Information. Estimated parameters for toluene-d_8 fit with extra lattice parameters (Table S1), SF-nSCFT density fields (Figure S1 – Figure S4), and Parameter uncertainty

correlation pair plot grids (Figure S5 – Figure S11) (PDF document.) NR and SANS data, along with Python scripts to fit and plot the data (ZIP archives.) This material is available free of charge via the Internet at http://pubs.acs.org.

Author information

Corresponding Author

*E-mail: beers@nist.gov

Author Contributions

The manuscript was written through contributions of all authors. All authors have given approval to the final version of the manuscript.

Funding Sources

Richard Sheridan wishes to acknowledge postdoctoral research support from the National Research Council Research Associateship Program.

Notes

The authors declare no competing financial interest. Certain commercial equipment, instruments, or materials are identified in this paper in order to specify the experimental procedure adequately. Such identification is not intended to imply recommendation or endorsement by the National Institute of Standards and Technology, nor is it intended to imply that the materials or equipment identified are necessarily the best available for the purpose.

Appendix

Scheutjens-Fleer numerical self-consistent field theory

Formalism

In this work we model the configurations of our end-tethered polymer film using the Scheutjens-Fleer numerical self-consistent field theory (SF-nSCFT) for polydisperse chains in a monomeric solvent as developed by de Vos and Leermakers.[33] Our implementation of the formalism differs only in that we re-introduce the effects of solvent quality χ and surface interaction χ_s into the segment Boltzmann weighting factor $G(z)$:

$$G(z) = \big(1 - \phi(z)\big)e^{-2\chi\langle\phi(z)\rangle - \delta_z\chi_s} \quad (5)$$

as done in the earlier work of Cosgrove.[32] In Eq 5, $\phi(z)$ is the volume fraction of polymer segments in layer z, δ_z is the Kronecker delta, indicating that the surface interaction potential is only applied in the first layer, and angle brackets indicate a contact-average. On a cubic lattice, the angle bracket notation expands to:

$$\langle f(z)\rangle = \tfrac{1}{6}\big(f(z-1) + 4f(z) + f(z+1)\big) \quad (6)$$

The partition function for each chain is found through the numerical solution of the Edwards diffusion equation,[43] which is done in the case of this formalism by integration over regular steps on a lattice. This integration is efficiently computed on a cubic lattice in terms of a recurrence relation:

$$G(z,s) = G(z)\langle G(z,s-1)\rangle \quad (7)$$

$G(z,s)$ is the Boltzmann weight corresponding to the presence of chain segment number s existing in lattice layer z out of a total L layers. Equation 7 can be interpreted as a Markov chain model: The frequency with which segment s will exist in layer z is equal to the frequency that segment $s-1$ was in an adjacent lattice cell times the statistical weight of any segment existing in layer z. The tethering of the chains is indicated by the boundary condition of this propagator: a free chain propagator begins with the placement of a lone lattice segment on the lattice, that is

$G(z,0) = G(z)$, whereas a tethered chain propagator begins $G(z,0) = \delta_z G(z)$, indicating every chain begins at the surface layer.

We model our polydispersity with the same Schultz-Zimm distribution, and use the same efficient computational scheme to calculate polymer volume fraction $\phi(z)$ in polydisperse systems as de Vos,[33] via the composition law:

$$\phi(z) = \frac{1}{G(z)} \sum_s G_{\text{ta}}(z,s) G_{\text{free}}(z, N_k \geq s) \qquad (8)$$

In Eq 8, $G_{\text{ta}}(z,s)$ is the forward tethered chain propagator and $G_{\text{free}}(z, N_k \geq s)$ is the backward free chain-end propagator for polydisperse systems of Roefs et al.[44] As we have an expression for $\phi(z)$ in terms of $G(z)$, and an expression for $G(z)$ in terms of $\phi(z)$, the formalism can be solved in terms of the fixed point ϕ_{f} of:

$$\phi\big(G(\phi_{\text{f}})\big) = \phi_{\text{f}} \qquad (9)$$

a system of L simultaneous, implicit, nonlinear equations, one for each layer, to be solved numerically. This route to numerical solution is an idiosyncrasy of two-component systems with a monomeric solvent, but was the first route proposed by Scheutjens and Fleer.[25] For a full background on the derivation of the statistical mechanics of the formalism and more general methods for solution, consult Evers et al.[45–47] or the textbook of Fleer et al.[27]

As a lattice theory, we must scale the dimensionless parameters that describe the system on the lattice appropriately back into real space. Each lattice element describes a volume of polymer segments roughly equivalent to a Kuhn length, or an equivalent volume of solvent molecules. Two numbers fully specify the configuration of end-tethered linear chains on the lattice: N_{l}, the number-average number of segments per lattice chain, and $\bar{\sigma}$, the fraction of surface sites occupied by a tethered chain end. N_{l} is straightforward to calculate from the number-average molecular mass of the real chains M_{n} using:

$$N_l = \frac{M_n}{m_l} \qquad (10)$$

given m_l, the mass of a lattice segment. $\bar{\sigma}$ can be calculated from N_l:

$$\bar{\sigma} = \frac{h_{dry}}{N_l l_l} \qquad (11)$$

using the dry thickness of the real film h_{dry} and the length of a lattice layer l_l. The parameters m_l and l_l can be calculated from measurements of the dimensions of real chains by asserting the equivalence of the unperturbed contour length and radius of gyration of the real chain and the lattice chain.[27] For polystyrene, we calculated the values m_l = 590 g/mol and l_l = 14.2 Å. The interaction parameters χ and χ_s map to slightly different specific enthalpies depending on the value of the lattice parameters. We intentionally ignore this effect, as the measured parameter estimates are in reality only effective values that contain contributions from entropic and virial terms which we also ignore. For the purposes of this study, these effective values are expected to scale properly when applied to critical phenomena such as theta and surface adsorption transitions.

Algorithmic considerations

An important feature of our SF-nSCFT implementation is that it is designed to have its parameters optimized algorithmically to fit the data we have collected. This requires a level of speed and robustness that was not obtained in the methods reported in the earlier literature. For even modest polymer lengths, the number of layers L is large enough to consider the solution of eq 9 to be a large-scale problem. Among the various large-scale solvers available, the Jacobian-free Newton-Krylov[48] solver provided by SciPy[49] in its optimize package provided acceptable performance when using GMRES as the internal Krylov linear solver method.[50] However, the convergence of the solver demonstrated sensitivity to the choice of input parameters and initial state. In other words, for some values of h_{dry}, χ and χ_s, the system would not converge without a

sufficiently good guess of $\phi(z)$. Since the optimization algorithm can input almost any combination of parameters and has no ability to guess $\phi(z)$, it became necessary to wrap the solver in two layers that can provide this information.

The outer wrapper caches a number of previously-calculated parameter-solution pairs. These cached points in parameter space are compared to the current parameters and the solution corresponding to the closest cached parameters (in terms of the L_2 norm of their difference vector) is selected as an initial guess. The solver is allowed to attempt a severely limited number of iterations. Then, either a solution at the point in parameter space is returned and cached, or an error is raised which triggers an algorithm to find a "nearby" point that will converge. This process is bootstrapped by priming the cache with a solution at a point that converges easily from a naïve initial guess. We borrow the backtracking linesearch concept from optimization theory and try points along the line between the cached and desired parameters, first the full distance, then half the distance, and so on, until the $\phi(z)$ at the cached point is within the basin of attraction for the solution field $\phi(z)$ at the intermediate set of parameters and the solver converges. This should work as long as eq 9 is continuous in terms of the parameters and the solution field, which appears to be the case for our system. The algorithm then walks along the line in parameter space, recursively applying the backtracking linesearch strategy along these smaller steps until finally reaching the solution to the field equations at the currently desired parameters. We have found this strategy to be successful for $\chi < 1.5$ and $\chi_s < 1$.

The inner wrapper resizes the lattice, since the number of lattice layers used at one solution may not be appropriate for another. When there are insufficient layers, the system simulated is actually the squeezing of an end-tethered polymer film between two plates. Thus, the layers must be far enough apart that the chains do not "see" the end of the lattice. If the solver produces a

solution where the volume fraction of polymer in the last layer is above a set tolerance, the array holding the solution is extended by a percentage and fed back into the solver. This is repeated until the tolerance criterion is met. The geometric growth tends to overshoot, so after this process the extra layers below the volume fraction threshold are dropped to save memory and processing time.

DREAM optimization algorithm

DiffeRential Evolution Adaptive Metropolis (DREAM) optimization is a Markov chain Monte Carlo based algorithm for function minimization.[51] Although it expends more function evaluations to locate an optimum as compared to the Levenberg-Marquardt method or other optimization algorithms, it is more robust to avoiding shallow local minima and provides Bayesian, empirical estimates of parameter uncertainty and correlation which fully propagate all uncertainty in the data through the model. In this paper, we reported the standard deviation of the values present in the annealed portion of the Markov chains as our estimate of parameter uncertainty, that is, the precision of our fit given the SF-nSCFT model and the specified parameter inputs. The standard deviation is only an approximation of the parameter uncertainty unless the parameters are perfectly uncorrelated. The true parameter uncertainty can be diagnosed by observing the Markov chain data in the form of a pair plot grid, which plots the values of each pair of parameters against each other at each point of the chain. These are presented in the Supporting Information. The DREAM algorithm cannot, however, speak to the accuracy of the parameter estimates in the face of model selection or experimental error.

References

(1) Nie, Z.; Kumacheva, E. Patterning Surfaces with Functional Polymers. *Nat. Mater.* **2008**, *7* (4), 277–290.

(2) Vladkova, T. G. Surface Engineered Polymeric Biomaterials with Improved Biocontact Properties. *Int. J. Polym. Sci.* **2010**, *2010*, 1–22.

(3) Wei, Q.; Becherer, T.; Angioletti-Uberti, S.; Dzubiella, J.; Wischke, C.; Neffe, A. T.; Lendlein, A.; Ballauff, M.; Haag, R. Protein Interactions with Polymer Coatings and Biomaterials. *Angew. Chemie Int. Ed.* **2014**, *53* (31), 8004–8031.

(4) Belenky, B. G.; Gankina, E. S.; Tennikov, M. B.; Vilenchik, L. Z. Fundamental Aspects of Adsorption Chromatography of Polymers and Their Experimental Verification by Thin-Layer Chromatography. *J. Chromatogr. A* **1978**, *147* (0), 99–110.

(5) Cohen Stuart, M. A.; Huck, W. T. S.; Genzer, J.; Müller, M.; Ober, C. K.; Stamm, M.; Sukhorukov, G. B.; Szleifer, I.; Tsukruk, V. V; Urban, M.; et al. Emerging Applications of Stimuli-Responsive Polymer Materials. *Nat. Mater.* **2010**, *9* (2), 101–113.

(6) Sohn, B. H.; Seo, B. H. Fabrication of the Multilayered Nanostructure of Alternating Polymers and Gold Nanoparticles with Thin Films of Self-Assembling Diblock Copolymers. *Chem. Mater.* **2001**, *13* (5), 1752–1757.

(7) Pasch, H. Chromatographic Investigations of Macromolecules in the Critical Range of Liquid Chromatography: 3. Analysis of Polymer Blends. *Polymer* **1993**, *34* (19), 4095–4099.

(8) Guttman, C. M.; Di Marzio, E. A.; Douglas, J. F. Influence of Polymer Architecture and Polymer−Surface Interaction on the Elution Chromatography of Macromolecules through a Microporous Media. *Macromolecules* **1996**, *29* (17), 5723–5733.

(9) Guttman, C. M.; Snyder, C. R.; Di Marzio, E. A. A Simple Method for Complex Monomer Creation in the Matrix Method for the Statistics and Thermodynamics of a Confined Polymer Chain. *Macromolecules* **2015**, *48* (3), 863–870.

(10) Snyder, C. R.; Guttman, C. M.; Di Marzio, E. A. Exact Solution of the Thermodynamics and Size Parameters of a Polymer Confined to a Lattice of Finite Size: Large Chain Limit. *J. Chem. Phys.* **2014**, *140* (3), 34905.

(11) DiMarzio, E. A.; Rubin, R. J. Adsorption of a Chain Polymer between Two Plates. *J. Chem. Phys.* **1971**, *55* (9), 4318.

(12) Casassa, E. F. Theoretical Models for Peak Migration in Gel Permeation Chromatography. *J. Phys. Chem.* **1971**, *75* (26), 3929–3939.

(13) Pasch, H.; Brinkmann, C.; Gallot, Y. Chromatographic Investigations of Macromolecules in the Critical Range of Liquid Chromatography: 4. Analysis of Poly(styrene-B-Methyl Methacrylate). *Polymer* **1993**, *34* (19), 4100–4104.

(14) Pasch, H.; Gallot, Y.; Trathnigg, B. Chromatographic Investigations of Macromolecules in the Critical Range of Liquid Chromatography: 7. Analysis of the Poly(methyl Methacrylate) Block in Poly(styrene-Block-Methyl Methacrylate). *Polymer* **1993**, *34* (23), 4986–4989.

(15) Pasch, H. Liquid Chromatography at the Critical Point of Adsorption - A New Technique for Polymer Characterization. *Macromol. Symp.* **1996**, *110* (1), 107–120.

(16) Van der Beek, G. P.; Cohen Stuart, M. A.; Fleer, G. J.; Hofman, J. E. A Chromatographic Method for the Determination of Segmental Adsorption Energies of Polymers. Polystyrene on Silica. *Langmuir* **1989**, *5* (5), 1180–1186.

(17) Vander Linden, C.; Van Leemput, R. Adsorption Studies of Polystyrene on Silica I. Monodisperse Adsorbate. *J. Colloid Interface Sci.* **1978**, *67* (1), 48–62.

(18) Cosgrove, T. Volume-Fraction Profiles of Adsorbed Polymers. *J. Chem. Soc. Faraday Trans.* **1990**, *86* (9), 1323.

(19) Cosgrove, T.; Crowley, T. L.; Ryan, K.; Webster, J. R. P. The Effects of Solvency on the Structure of an Adsorbed Polymer Layer and Dispersion Stability. *Colloids and Surfaces* **1990**, *51*, 255–269.

(20) Mansfield, T. L.; Iyengar, D. R.; Beaucage, G.; McCarthy, T. J.; Stein, R. S.; Composto, R. J. Neutron Reflectivity Studies of End-Grafted Polymers. *Macromolecules* **1995**, *28* (2), 492–499.

(21) Milner, S. T.; Witten, T. A.; Cates, M. E. A Parabolic Density Profile for Grafted Polymers. *Europhys. Lett.* **1988**, *5* (5), 413–418.

(22) Skvortsov, A. M.; Pavlushkov, I. V.; Gorbunov, A. A.; Zhulina, E. B.; Borisov, O. V.; Pryamitsyn, V. A. Structure of Densely Grafted Polymeric Monolayers. *Polym. Sci. U.S.S.R.* **1988**, *30* (8), 1706–1715.

(23) Zhulina, E. B.; Borisov, O. V.; Pryamitsyn, V. A.; Birshtein, T. M. Coil-Globule Type Transitions in Polymers. 1. Collapse of Layers of Grafted Polymer Chains. *Macromolecules* **1991**, *24* (1), 140–149.

(24) Adamuţi-Trache, M.; McMullen, W. E.; Douglas, J. F. Segmental Concentration Profiles of End-Tethered Polymers with Excluded-Volume and Surface Interactions. *J. Chem. Phys.* **1996**, *105* (11), 4798.

(25) Scheutjens, J. M. H. M.; Fleer, G. J. Statistical Theory of the Adsorption of Interacting Chain Molecules. 1. Partition Function, Segment Density Distribution, and Adsorption Isotherms. *J. Phys. Chem.* **1979**, *83* (12), 1619–1635.

(26) Scheutjens, J. M. H. M.; Fleer, G. J. Statistical Theory of the Adsorption of Interacting Chain Molecules. 2. Train, Loop, and Tail Size Distribution. *J. Phys. Chem.* **1980**, *84* (2), 178–190.

(27) Fleer, G. J.; Cohen Stuart, M. A.; Scheutjens, J. M. H. M.; Cosgrove, T.; Vincent, B. *Polymers at Interfaces*; Chapman & Hall: London, 1993.

(28) Chennevière, A.; Drockenmuller, E.; Damiron, D.; Cousin, F.; Boué, F.; Restagno, F.; Léger, L. Quantitative Analysis of Interdigitation Kinetics between a Polymer Melt and a Polymer Brush. *Macromolecules* **2013**, *46* (17), 6955–6962.

(29) Jiang, N.; Shang, J.; Di, X.; Endoh, M. K.; Koga, T. Formation Mechanism of High-Density, Flattened Polymer Nanolayers Adsorbed on Planar Solids. *Macromolecules* **2014**, *47* (8), 2682–2689.

(30) Kienzle, P. A.; O'Donovan, K. V.; Ankner, J. F.; Berk, N. F.; Majkrzak, C. F. Reflpak. 2015.

(31) Kienzle, P. A.; Krycka, J.; Patel, N.; Sahin, I. Refl1D. University of Maryland: College Park, MD 2011.

(32) Cosgrove, T.; Heath, T.; Van Lent, B.; Leermakers, F. A. M.; Scheutjens, J. M. H. M. Configuration of Terminally Attached Chains at the Solid/solvent Interface: Self-Consistent Field Theory and a Monte Carlo Model. *Macromolecules* **1987**, *20* (7), 1692–1696.

(33) de Vos, W. M.; Leermakers, F. A. M. Modeling the Structure of a Polydisperse Polymer Brush. *Polymer* **2009**, *50* (1), 305–316.

(34) Kline, S. R. Reduction and Analysis of SANS and USANS Data Using IGOR Pro. *J. Appl. Crystallogr.* **2006**, *39* (6), 895–900.

(35) Butler, P.; Alina, G.; Hernandez, R. C.; Doucet, M.; Jackson, A.; Kienzle, P.; Kline, S.; Zhou, J. SASView for Small Angle Scattering Analysis.

(36) Hammouda, B. SANS from Homogeneous Polymer Mixtures: A Unified Overview. In *Polymer Characteristics*; Springer-Verlag: Berlin/Heidelberg, 1993; pp 87–133.

(37) Tidswell, I. M.; Ocko, B. M.; Pershan, P. S.; Wasserman, S. R.; Whitesides, G. M.; Axe, J. D. X-Ray Specular Reflection Studies of Silicon Coated by Organic Monolayers (Alkylsiloxanes). *Phys. Rev. B* **1990**, *41* (2), 1111–1128.

(38) Abelès, F. La Théorie Générale Des Couches Minces. *J. Phys. le Radium* **1950**, *11* (7), 307–309.

(39) Cotton, J. P. Experimental Determination of the Temperature–concentration Diagram of Flexible Polymer Solutions by Neutron Scattering. *J. Chem. Phys.* **1976**, *65* (1976), 1101.

(40) Gallagher, P. D.; Satija, S. K.; Karim, A.; Douglas, J. F.; Fetters, L. J. Swelling of a Polymer Brush by a Poor Solvent. *J. Polym. Sci. Part B Polym. Phys.* **2004**, *42* (22), 4126–4131.

(41) Sun, S.-T.; Nishio, I.; Swislow, G.; Tanaka, T. The Coil–globule Transition: Radius of Gyration of Polystyrene in Cyclohexane. *J. Chem. Phys.* **1980**, *73* (12), 5971.

(42) Whitmore, M. D.; Grest, G. S.; Douglas, J. F.; Kent, M. S.; Suo, T. End-Anchored Polymers in Good Solvents from the Single Chain Limit to High Anchoring Densities. *J. Chem. Phys.* **2016**, *145* (17), 174904.

(43) Edwards, S. F. The Statistical Mechanics of Polymers with Excluded Volume. *Proc. Phys. Soc.* **1965**, *85* (4), 613–624.

(44) Roefs, S. P. F. M.; Scheutjens, J. M. H. M.; Leermakers, F. A. M. Adsorption Theory for Polydisperse Polymers. *Macromolecules* **1994**, *27* (17), 4810–4816.

(45) Evers, O. A.; Scheutjens, J. M. H. M.; Fleer, G. J. Statistical Thermodynamics of Block Copolymer Adsorption. 1. Formulation of the Model and Results for the Adsorbed Layer Structure. *Macromolecules* **1990**, *23* (25), 5221–5233.

(46) Evers, O. A.; Scheutjens, J. M. H. M.; Fleer, G. J. Statistical Thermodynamics of Block Copolymer Adsorption. Part 2. Effect of Chain Composition on the Adsorbed Amount and Layer Thickness. *J. Chem. Soc. Faraday Trans.* **1990**, *86* (9), 1333.

(47) Evers, O. A.; Scheutjens, J. M. H. M.; Fleer, G. J. Statistical Thermodynamics of Block Copolymer Adsorption. 3. Interaction between Adsorbed Layers of Block Copolymers. *Macromolecules* **1991**, *24* (20), 5558–5566.

(48) Knoll, D. A.; Keyes, D. E. Jacobian-Free Newton–Krylov Methods: A Survey of Approaches and Applications. *J. Comput. Phys.* **2004**, *193* (2), 357–397.

(49) Jones, E.; Oliphant, T.; Peterson, P.; Others. SciPy: Open Source Scientific Tools for Python.

(50) Kelley, C. *Iterative Methods for Linear and Nonlinear Equations*; Society for Industrial and Applied Mathematics: Philadelphia, 1995.

(51) Vrugt, J. A.; ter Braak, C. J. F.; Diks, C. G. H.; Robinson, B. A.; Hyman, J. M.; Higdon, D. Accelerating Markov Chain Monte Carlo Simulation by Differential Evolution with Self-Adaptive Randomized Subspace Sampling. *Int. J. Nonlinear Sci. Numer. Simul.* **2009**, *10* (3).

(51) Kent, M. S. A Quantitative Study of Tethered Chains in Various Solution Conditions Using Langmuir Diblock Copolymer Monolayers. *Macromol Rapid Commun.* **2000**, *21* (6), 243-270.

Table of Contents Graphic